Research Article Vol. 4, No. 6 / 15 Jun 2025 / Optics Continuum 1198
OPTICS CONTINUUM

Three-mode photonic lanterns: comprehensive analysis from theory to experiments

RODRIGO ITZAMNÁ BECERRA-DEANA,[1,2] RAPHAEL MALTAIS-TARIANT,[1,3] GUILLAUME RAMADIER,[1] MARTIN POINSINET DE SIVRY-HOULE,[1] STÉPHANE VIRALLY,[1] CAROLINE BOUDOUX,[1,2,3] AND NICOLAS GODBOUT[1,2,*]

[1] Polytechnique Montréal, 2500 Chemin de Polytechnique, Montréal, QC H3T 1J4, Canada
[2] Castor Optics, 361 Boulevard Montpellier, Saint-Laurent, QC H4N 2G6, Canada
[3] CHU Sainte-Justine, 3175 Chemin de la Côte Sainte-Catherine, Montréal, QC H3T 1C5, Canada
[*] nicolas.godbout@polymtl.ca

Abstract: The design space for photonic lanterns is large and complex, making it challenging to identify optimal parameters to achieve specific performances, such as coupling, bandwidth, and insertion loss. Effectively navigating this space requires modeling tools capable of extracting the most characterizing parameters. This work contrasts theoretical modeling with experimental realizations of the four possible types of 3×1 photonic lanterns using double-clad fibers, covering a spectrum from conventional to hybrid to mode-specific configurations. This work highlights the experimental characteristics of each photonic lantern.

© 2025 Optica Publishing Group under the terms of the Optica Open Access Publishing Agreement

1. Introduction

Photonic lanterns (PLs) are $N \times 1$ transverse-mode division multiplexers/de-multiplexers composed of N single-mode fibers fused together into a few-mode waveguide [1]. They are typically fabricated by heating and tapering a bundle of N fibers before cleaving the resulting fused section, acting as a few-mode segment. PLs are used in a variety of applications including telecommunications [2–9], lasers [10,11], astrophysics [12,13], sensing [14,15], orbital angular momentum mode generation [16], efficient collection of light [17], and biomedical imaging [18–21].

The characteristics of PLs vary greatly depending on the fiber configuration and type within the bundle. In general, their behavior can be sorted into three main categories, which we herein call conventional, mode-selective, and hybrid. Conventional PLs are fabricated from N identical single-mode fibers [2,22,23] and equally couple each fiber's fundamental modes to the transverse modes of the multimode section. Conversely, they enable the equipartite collection of the amplitudes of the transverse modes into all N single-mode outputs without distinction between each port. This behavior differs from that of so-called mode-selective photonic lanterns (MSPLs), consisting of N different fibers acting as mode sorters whereby each transverse mode of the few-mode section is selectively coupled to a specific single-mode fiber [20,24–26]. MSPLs usually have high modal isolation, and their operation is typically wavelength-independent, up to a bandwidth of 500 nm [27]. The hybrid type—also called semi-selective or group-mode-selective [28–30]—refers to PLs behaving in between the conventional and mode-selective types.

The plurality of PL designs provides a large design space. Computational electromagnetics (CEM) methods [31,32] such as finite-difference time-domain (FDTD) and the method of moments (MoM) are often used when no simple closed-form solutions to Maxwell's equations exist. Recent studies have demonstrated that Coupled-mode theory (CMT) serves as an effective implementation for simulating guided waves in complex structures [33–36]. This method aptly captures the complexities of electromagnetic field dynamics, transforming it into a more

#564008 https://doi.org/10.1364/OPTCON.564008
Journal © 2025 Received 2 Apr 2025; revised 3 May 2025; accepted 5 May 2025; published 4 Jun 2025

OPTICS CONTINUUM

manageable eigenvalue problem. Our group accomplished this through a Python package named SuPyMode [36].

CMT modeling of PLs allows observing the spectrum of behaviors exhibited by various types of PLs, particularly those stemming from symmetry-breaking fiber arrangements, which is well represented by eigenmode decomposition. However, most of the existing simulators operate under ideal conditions. While they provide valuable approximations, fully understanding a device's performance requires actual fabrication and characterization to ascertain the modal coupling and wavelength response, which are crucial for implementation in various fields.

In this study, we first briefly introduce adiabatic criteria and the logarithmic taper slope associated with a particular fabrication sequence. We combine these two concepts to determine the best parameters for a given component. We then compare theoretical predictions with actual fabricated components of each type of photonic lantern, demonstrating their different performances at each port over a wide bandwidth and their optical profiles. We emphasize the significant differences in the experimental behaviors of components that may seem very similar at first but have distinct internal symmetries.

2. Modeling tools

The main characteristics of PLs can be determined theoretically by comparing the inter-modal adiabatic criteria to the logarithmic slope of the taper. We briefly introduce those two concepts and their relation to the final characteristics of the devices.

2.1. Adiabatic criterion

The design of PLs involves many parameters, including the types of fibers, stacking arrangement, amount of initial fusion, and tapering profile. All of these parameters directly influence the adiabatic criteria, which ultimately determine if and how a device can be fabricated.

In CMT, the adiabatic criterion $\overline{\alpha}_{ij}$ between two transverse eigenmodes i and j is a quantity with units of the inverse of a length. It depends only on two properties of the modes in question: their propagation constants β_i and β_j, and their normalized amplitude profiles Ψ_i and Ψ_j [33,34,36]. At any position z along the taper, these can be calculated from the transverse refraction index map $n_0(x, y, z)$ of the fused fiber bundle. The package that we used in this study, SuPyMode [36,37], determines this map from homotetic transformation of the cross-sectional map $n_0(x, y)$ of the fused fiber bundle before tapering. A typical map is shown in Fig. 1(a). The homotetic ratio $\boldsymbol{I}(z)$ between the length of any line segment on the fiber cross-section before and after tapering at any particular position z is called the inverse taper ratio (ITR).

2.2. Logarithmic slope

By definition, the logarithmic slope of the taper at any position z is the logarithmic derivative $\frac{1}{\boldsymbol{I}}\frac{\partial}{\partial \boldsymbol{I}}$ of the ITR at that position. his logarithmic slope, also known as the taper shape, is controlled by the scanning and pulling motors during the fabrication process. The specific shape of the taper is determined by theoretical considerations [38]. Each step of the sequence consists of heating a section of the bundle, at each point increasing or decreasing the length of the heated section to the value $L = L_0 + \alpha\,\delta z$, where L_0 is the original heating length of the section, and δz is the current elongation of the section. The coefficient α is unitless and ranges from -1 to $+1$. A positive value of α indicates that the length of the heated section increases as the step progresses. In turn, a negative value of α indicates that the length of the heated section decreases throughout the step. The ITR is fully determined by the ensemble of parameters L_0 and α [38] for each step of the sequence.

OPTICS CONTINUUM

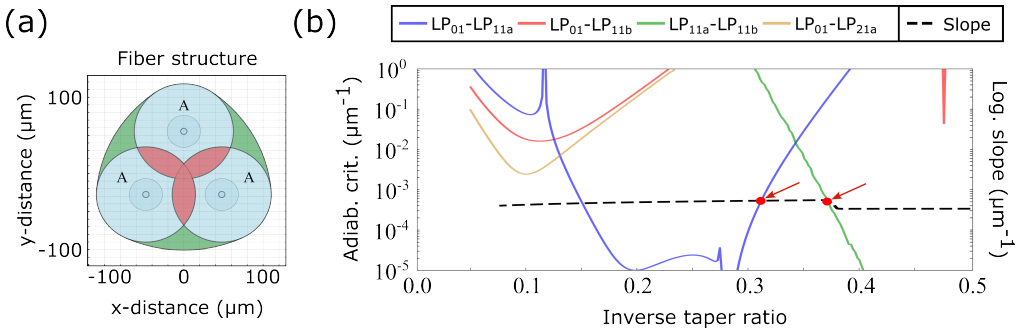

Fig. 1. Simulation of a three-mode structure using SuPyMode. (a) Cross-sectional map of refraction indices after fusion initial fusion of the three-fiber bundle. (b) Adiabatic criteria for each mode pair (solid lines) and logarithmic slope of the taper (dashed line) for a given fabrication sequence. The arrows indicate crossings that potentially imply coupling between specific modes, although additional judgment must be applied (see text and supplementary material-Supplement 1).

2.3. Coupling threshold

The threshold between inter-modal coupling and inter-modal isolation is determined for each pair of modes (i, j) by comparing the adiabatic criterion for the pair to the logarithmic slope determined by the fabrication sequence. Specifically, the condition for inter-modal isolation is $\frac{1}{\boldsymbol{I}}\frac{\partial \boldsymbol{I}}{\partial z} \leq \overline{\alpha}_{ij}$ over the full length of the taper.

In addition, a taper is called adiabatic when inter-modal isolation is maintained for all pairs of modes guided by the structure, or

$$\frac{1}{\boldsymbol{I}(z)}\frac{\partial \boldsymbol{I}(z)}{\partial z} \leq \min_{(i,j)} \overline{\alpha}_{ij}(z) \quad \forall z. \tag{1}$$

Thus, one of the primordial modeling tools for the design of PLs is a graph comparing all relevant adiabatic criteria to the logarithmic slope determined by the fabrication sequence. An example of such a graph is shown in Fig. 1(b). This figure shows adiabatic criteria and logarithmic slope values for a specific fabrication sequence as a function of ITR rather than the longitudinal position z of the taper. This improves the readability of the graph, as tapers often feature sections with constant ITRs. The features shown in this particular graph will be reproduced and explained in more details below as it pertains to a case studied in this paper. The supplementary material (Supplement 1) provides a deeper dive into these types of graphs and all the information that can be extracted from them.

3. Methodology

In the next section, we highlight the three main fiber configurations and fabrication and characterization of 3×1 components as they already exhibit the full variety of PLs, from conventional to mode-specific and anything in between.

3.1. Fiber configurations

We compare three main types of PLs: devices made of three identical fibers should result in conventional PLs; devices made of three different fibers should result in MSPLs; devices made of two different types of fibers should be hybrids.

Figure 2(a) shows the three main fiber configurations: AAA (three identical fibers), ABC (all different fibers), and ABB (two different types of fibers, each supporting a different mode group).

OPTICS CONTINUUM

For practicality, we use double-clad fibers with single-mode compatibility at 1550 nm. All fibers feature a 9 μm single-mode core and similar numerical apertures (NAs) ~ 0.13. They also feature similar first cladding NAs ~ 0.12 and vary only by first cladding diameters, with respective sizes of 19.6, 32.3, and 42 μm (custom-designed, 2058I1, 2058K1, and 2058J1, Université Laval, Prof. Messaddeq, QC, CA).

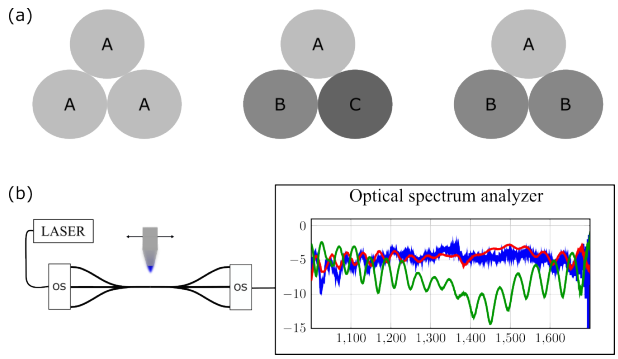

Fig. 2. Three-mode structures and fabrication process. (a) Three different structures in which each letter represents a type of fiber; AAA uses three identical fibers, ABC uses different fibers, and ABB uses two types of fibers. (b) Schematic diagram of the fusion and tapering station with a heating torch, an illuminating laser, two optical switches (OS), and an optical spectrum analyzer.

3.2. Fabrication and characterization

Before the fusion-taper procedure, all fiber bundles were constrained inside a synthetic fused silica capillary tube (CV1012, Vitrocom, NJ, USA). In-situ, real-time monitoring of the components during fusion and tapering allows to observe and potentially remedy any anomalous loss or coupling between modes [39]. The bundles were clamped to an in-house built setup that allows for fusion and tapering using a mobile torch while pulling on each side. For better comparison, all devices for this study were fabricated using the same sequence, i.e. the same α and L_0 values at all ITRs. In addition, the same characterization setup was used every time. Figure 2(b) shows the in-situ optical characterization system. It starts with a broadband laser source (Energetiq Fiber Coupled Laser-Driven Light Source, model EQ-99, MA, USA) that injects light into a first, in-house built, optical switch (OS) spliced to the input single-mode fibers of the PLs. At the output, a second OS allows the monitoring of each port through an optical spectrum analyzer (OSA, model AQ6317, Ando, Japan). Power transfer is measured by injecting light into one input port and measuring the output across three ports. Additionally, the excess loss is calculated by summing the ratios of all power outputs. After fabrication, the few-mode tapered section was cleaved in the center, producing two identical PLs. Optical far-field profiles were obtained by illuminating each port sequentially with a source operating at 1300 nm (HP 8153ASM, Hewlett-Packard, CA, USA) and capturing the image with an infrared camera (SU320KTS-1.7RT, Goodrich, NJ, USA).

4. Results

The following subsections outline the key characteristics of each type of 3-mode PL. This includes a theoretical analysis of the fabrication process, followed by experimental results concerning the final structure's power transfer and the component's optical profile after it has been cleaved. This procedure is consistent across all components, allowing us to identify their main differences.

OPTICS CONTINUUM

4.1. Conventional photonic lanterns

Figure 3 shows the results for a type AAA component, conventional PLs, using three identical fibers (first cladding diameter of 42 μm). Figure 3(a) shows the adiabatic criteria (solid lines) and logarithmic slope (dashed line) calculated by SuPyMode. Two crossings of adiabatic criteria with the logarithmic slope are highlighted by arrows. They show large ranges of ITR for which the adiabatic criteria are below the logarithmic slope: between ~ 0.15 and ~ 0.32 for the LP_{01}-LP_{11a} pair, and above ~ 0.38 for the LP_{11a}-LP_{11b} pair. Those are the three guided modes in the few-mode section, and they are all coupled together via LP_{11a}. Hence, the expected behavior is a split of power between the three modes, independent of the illuminated port. In addition, the model predicts a quasi-lossless device when fabricated without defects because there is no crossing between any guided and unguided modes. This explanation is provided in more detail in Supplement 1. This is witnessed by the fact that the adiabatic criteria coupling the guided modes to the unguided modes of the few-mode section are all above the logarithmic slope curve.

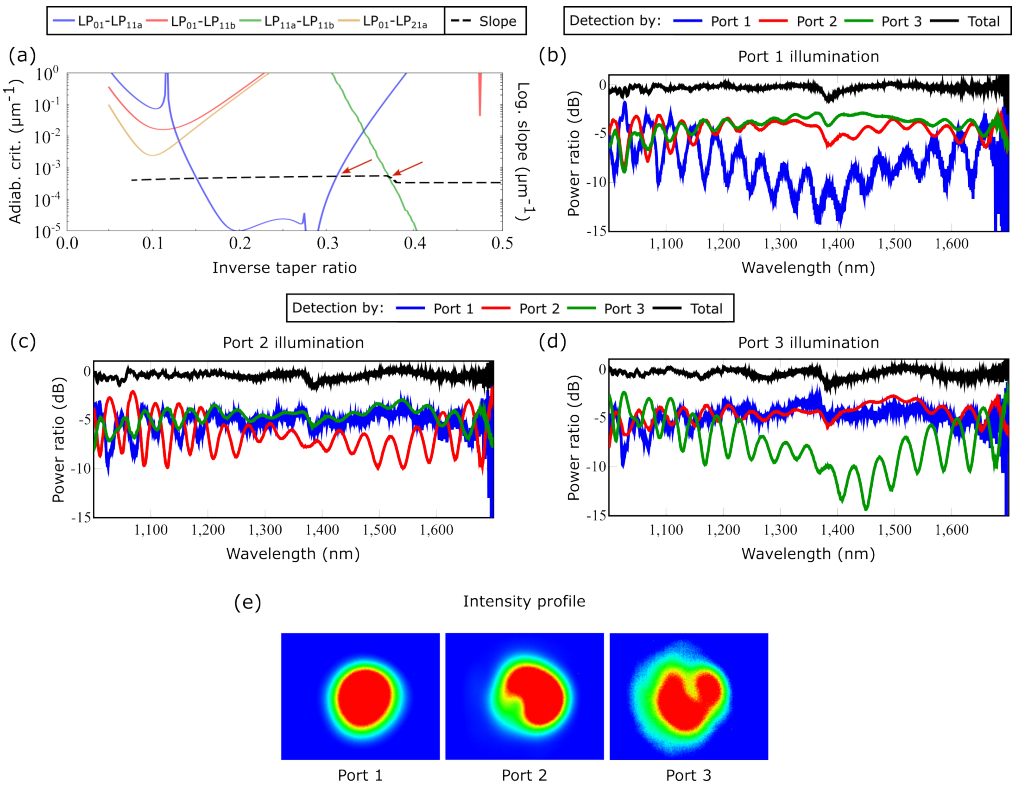

Fig. 3. AAA fiber configuration. (a) Adiabatic criteria for three identical (AAA) double-clad fibers with a 42 μm-diameter first cladding. The solid blue, red, and green lines show the criteria for each pair of guided modes (LP_{01}, LP_{11a} and LP_{11b}, respectively) in the few-mode tapered section of the device. The lowest adiabatic criterion for coupling between a guided and a non-guided mode (LP_{01} and LP_{21a} in this instance) is also shown. The dashed black curve corresponds to the logarithmic slope for the fabrication sequence. (b–d) Power ratio in each branch, with respect to the input power, after fusion and tapering but before cleaving (branch 1 in blue, 2 in red, 3 in green, total in black) when illuminating input 1 (b), input 2 (c), or input 3 (d), respectively. (e) Far-field optical profile of the few-mode structure after cleaving and illuminating each port.

OPTICS CONTINUUM

Although SuPyMode calculates a large amount of adiabatic criteria, for the sake of clarity, we only show the lowest of the guided-to-unguided pairs (between LP_{01} and LP_{21a}) in Fig. 3(a). A more detailed (and more cluttered) example of adiabatic criteria curves is provided as an example in the supplementary material (Supplement 1).

To ascertain the validity of the predictions from the model, we measured the ratio of power in each output, with respect to the power injected at each input, separately. This was done using the in-situ characterization setup at the end of the fusion and tapering process but before cleaving. The results are shown in Figs. 3(b–d). The power ratio of each branch with respect to the illumination power is color-coded: branch 1 is blue, 2 is red, and 3 is green). Excess loss at all wavelengths is shown as the black line. Illumination of branch 1 corresponds to Fig. 3(b), branch 2 to Fig. 3(c), and branch 3 to Fig. 3(d).

The three graphs show the expected strong coupling between all the ports. The ratio of power sent to the two non-illuminated branches is about −5 dB, or one-third, as expected. The strong oscillations on the power ratio of the illuminated branch are expected and are due to interference between the modes. They are highly dependent on the exact length of the tapered section and do not reflect actual coupling values in the final component (which will be cleaved in the middle of the tapered section). Only their average trend is relevant. That trend still shows some imperfections of the device, with slightly higher coupling to the non-illuminated branches and slightly higher excess loss (black line) at ∼ 1400 nm. This results in low ratios of power in the illuminating branch (down to less than 10% in two cases). However, the device displays low overall excess loss.

Finally, the far-field images of Fig. 3(e) reinforce the fact that the three modes LP_{01}, LP_{11a} and LP_{11b} are well mixed at the output. None of the images features well-defined transverse mode structures.

4.2. Mode-selective photonic lanterns

MSPLs are obtained with components that exhibit no coupling between modes. This can be slightly counter-intuitive in the realm of fiber-based components, which often rely on mode-coupling to exhibit interesting behaviors. In this case, however, it should be no real surprise as the idea is to segregate the transverse modes of the few-mode section to selectively direct them into three different single-mode fibers. This can be readily achieved by sufficiently breaking all the symmetries existing in the previous (AAA) configuration. Hence, mode-selectivity is achieved by using three sufficiently different fibers. In this study, we chose three different double-clad fibers (DCFs) with identical single-mode characteristics (see sub-section 3.1) and varying first-cladding diameters.

Simulations are displayed in Fig. 4(a). They indicate that there should be no coupling between modes. A notable feature, however, seems to suggest otherwise: a crossing of the adiabatic criterion between modes LP_{11a} and LP_{11b} at ∼ 0.23 ITR is highlighted by a red arrow in the graph. This is when additional judgment and experience are required in the interpretation. This type of very narrow and very abrupt decrease of an adiabatic criterion is usually spurious. It is an artifact that exists whenever two propagation constants β_i and β_j become equal. A good rule of thumb is to discard very narrow crossings in the graphs. In the end, the simulation suggests that a device fabricated with notable defects should be highly mode-selective and quasi-lossless.

Figures 4(b–d) show the power transfer for all illumination scenarios where the power remains mainly in the illuminated branch. Power transfers to the non-illuminated branches are minimal, below 10% for most wavelengths. Specifically, in Fig. 4(b), modal isolation between the LP_{01}-like mode and the two LP_{11}-like modes is shown to be above 20 dB for the range of 1200–1600 nm, and above 12 dB throughout. In Figs. 4(c–d), modal isolation between the two LP_{11} modes is shown to be above 10 dB from 1000–1600 nm. In general, isolation is lower, and excess loss is higher in the measured wavelength range. The effective operational range of these components

OPTICS CONTINUUM

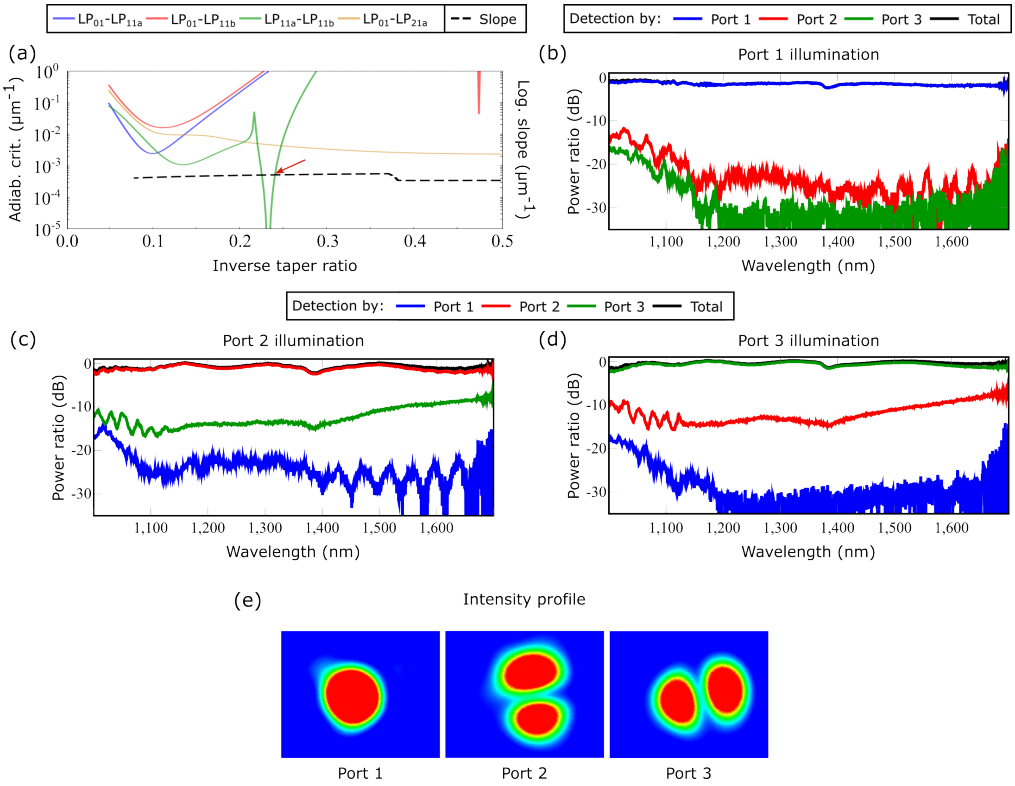

Fig. 4. ABC fiber configuration. (a) Adiabatic criteria for three different double-clad fibers with 42 (A-branch 1), 32.3 (B-branch 2), and 19.6 μm (C-branch 3) first cladding diameter, respectively. The solid blue, red, and green lines show the criteria for each pair of guided modes (LP_{01}, LP_{11a}, and LP_{11b}) in the few-mode tapered section of the device. The lowest adiabatic criterion for coupling between a guided and a non-guided mode (LP_{01} and LP_{21a} in this instance) is also shown. The dashed black curve corresponds to the logarithmic slope for the fabrication sequence. (b–d) Power ratio in each branch, with respect to the input power, after fusion and tapering but before cleaving (branch 1 in blue, 2 in red, 3 in green, total in black) when illuminating input 1 (b), input 2 (c), or input 3 (d), respectively. (e) Far-field optical profile of the few-mode structure after cleaving and illuminating each port.

remains very large, at around 500 nm. In addition, the fabricated device proves to be with low excess loss.

In contrast to the case of the conventional PL, the far-field images of Fig. 4(e) display the well-delineated shapes of the expected transverse modes that look like the LP_{01}, LP_{11a}, and LP_{11b}.

4.3. Hybrid photonic lanterns

Even with only three fibers in the bundle, devices can be made that will display behaviors between those of conventional and mode-selective components. An obvious way to achieve such behavior with 3×1 PLs is to use two different types of fibers. Here, we introduce two types of hybrid devices, which we call ABB and AAB, where A represents the fiber with the largest first cladding diameter. Interestingly, the two cases display rather different behaviors. A device of type ABB will segregate the LP_{01}-like mode from the twin LP_{11}-like modes, whereas a device of type AAB will hybridize the LP_{01}-like mode with one of the LP_{11}-like modes, while the other one will

OPTICS CONTINUUM

be segregated. Hence, already with 3 fibers, hybrid PLs components display a variety that can only grow with the number of fibers and can, in principle, be used to tailor devices to desired applications.

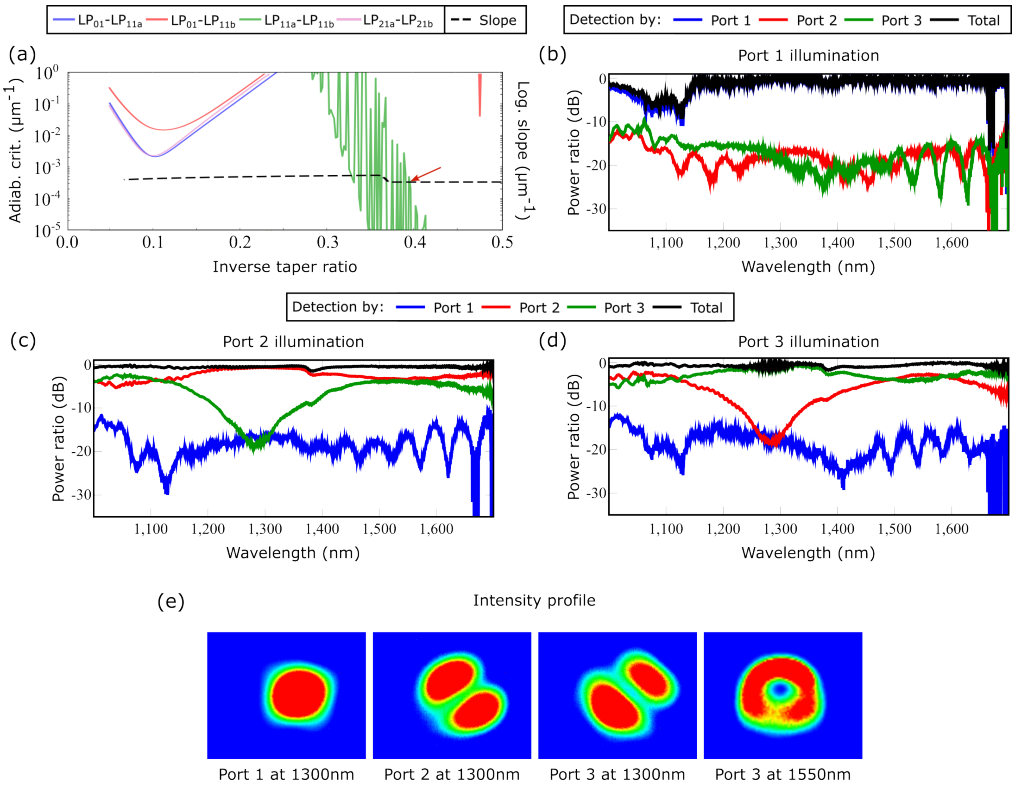

Fig. 5. ABB fiber configuration. (a) Adiabatic criteria for two different types of double-clad fibers with 42 (A-branch 1) and 32.3 (B-branches 2 and 3) first cladding diameter, respectively. The solid blue, red, and green lines show the criteria for each pair of guided modes (LP_{01}, LP_{11a}, and LP_{11b}) in the few-mode tapered section of the device. The dashed black curve corresponds to the logarithmic slope for the fabrication sequence. (b–d) Power ratio in each branch, with respect to the input power, after fusion and tapering but before cleaving (branch 1 in blue, 2 in red, 3 in green, total in black) when illuminating input 1 (b), input 2 (c), or input 3 (d), respectively. (e) Far-field optical profile of the few-mode structure after cleaving and illuminating each port. The first three images were obtained at 1300 nm. The last one is of port 3 at 1550 nm. It shows mixing between the two LP_{11}-like modes.

Figure 5(a) shows a range of ITRs above ~ 0.38 for which the adiabatic criterion between the twin LP_{11} modes is lower than the logarithmic slope curve. Hence, we can expect a hybridization of those modes and the segregation of the fundamental LP_{01}-like mode. The rapidly oscillating nature of the green adiabatic criterion curve reflects numerical instabilities caused by the degeneracy between the LP_{11} modes. Only the trend is helpful here. In contrast, the model does not predict any coupling between the fundamental mode LP_{01} and the twin LP_{11} modes. Nor does it predict any coupling between guided and unguided modes, which suggests that the particular fabrication sequence, absent defects, can produce a quasi-lossless device.

The experimental results are shown In Fig. 5(b-e). In Fig. 5(b), illumination through the first port, corresponding to the lone type A fiber and in principle to the fundamental LP_{01}-like mode, shows high isolation of that mode from the other two guided modes. This is close to the scenario

OPTICS CONTINUUM

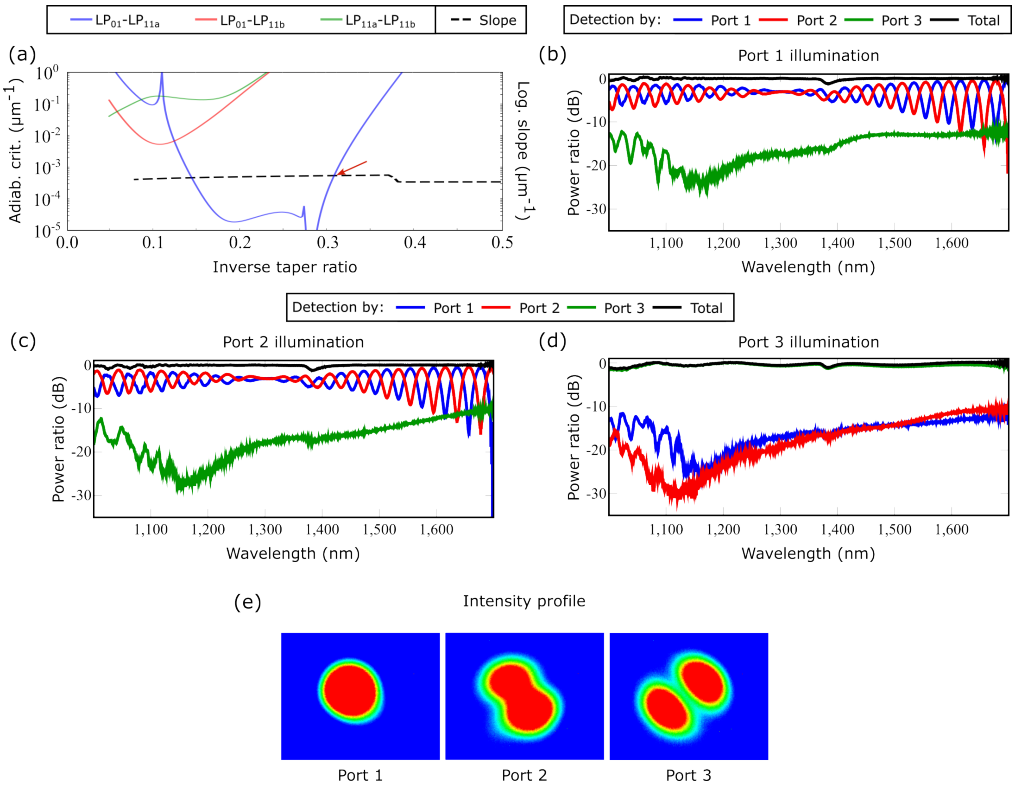

Fig. 6. AAB fiber configuration. (a) Adiabatic criteria for two different types of double-clad fibers with 42 (A-branches 1 and 2) and 32.3 (B-branch 3) first cladding diameter, respectively. The solid blue, red, and green lines show the criteria for each pair of guided modes (LP_{01}, LP_{11a}, and LP_{11b}) in the few-mode tapered section of the device. The dashed black curve corresponds to the logarithmic slope for the fabrication sequence. (b–d) Power ratio in each branch, with respect to the input power, after fusion and tapering but before cleaving (branch 1 in blue, 2 in red, 3 in green, total in black) when illuminating input 1 (b), input 2 (c), or input 3 (d), respectively. (e) Far-field optical profile of the few-mode structure after cleaving and illuminating each port.

OPTICS CONTINUUM

of Fig. 4(b), although in the case of this specific component, higher losses are observed below 1150 nm. In contrast, much higher power transfers exist between the LP_{11} branches, as shown in Figs. 5(c,d). A slow interferometric beating can erroneously lead to the impression that the coupling is highly dependent on the wavelength. This is not the case: coupling remains high throughout, and only the exact length of the tapered section dictates, through interference, how much power is found in each branch.

The first three images in Fig. 5(e) actually show strongly segregated LP_{11}-like modes, akin to the mode-selective case shown in Fig. 4(e). This is because the wavelength of the narrow-band illumination laser used for this characterization step, 1300 nm, is very close to a minimum of the hybridization between the LP_{11}-like modes. For this component, we also took a picture with illumination at 1550 nm (last image in Fig. 5(e)), which shows hybridization of the LP_{11}-like modes. Interestingly, the interference pattern strongly depends on the polarization state of the illumination laser, a feature that we intend to explore fully in the near future.

A configuration with two A-type fibers (42 μm first cladding diameter) and one B-type (32.3 μm first cladding diameter), or configuration AAB, is not an intuitively straightforward, as the fundamental mode will be hybridized with one of the LP_{11} modes, leaving the other segregated. In other words, the break in the physical symmetry does not correspond to the natural symmetry breaking of the mode structure. The results, shown in Fig. 6 are nonetheless enlightening and we include them here for completeness.

As shown in Fig. 6(a) there is a large region of ITRs, between ~ 0.15 and ~ 0.3, where the adiabatic criterion of the LP_{01}-LP_{11a} pair falls below the logarithmic slope curve. We can thus expect power transfers between the two modes while LP_{11b} remains segregated.

Figures 6(b,c) indeed show strong coupling between LP_{01} and LP_{11a}, while LP_{11b} is isolated. The rapid interferometric oscillations observed in these figures are highly dependent on the actual length of the tapered section, and only the average value is relevant. In contrast, illumination of the lone B-type fiber shows modal isolation greater than 10 dB throughout.

The optical profiles in the far field, shown in Fig. 6(e), are interesting. In particular, the second profile is clearly a superposition of the LP_{01} mode with one of the LP_{11} modes, while the last profile is purely LP_{11}-like. It is unclear if this feature could easily be exploited in an experiment.

5. Discussion

CMT gives rise to very useful modeling tools for the fabrication of complex devices such as PLs, as highlighted by the strong agreement between theory and experiment highlighted in this study. All simulations depict ideal scenarios, assuming no perturbation along the taper axis (dust, micro-bending, uniform fusion) and perfectly homothetic reduction of the taper. However, imperfections or mechanical flaws may arise during fabrication, leading to excess losses or power transfer in fibers that are supposed to exhibit high modal isolation. Therefore, it is essential to carefully characterize and monitor each PL type. Indeed, we showed that a comparison between adiabatic criteria and logarithmic slopes predicts the behaviors of various types of PLs. As with any modeling tool, however, informed judgment is required to interpret results adequately. For instance, the sudden but very brief plunge of an adiabatic criterion can mislead into thinking that coupling will occur when actual modes remain segregated. Such a spurious signal which occurs only when a criterion lies below the logarithmic slope over a large range of ITRs must be distinguished from actual coupling. The simulations were used as a guideline since achieving ideal scenarios during the fabrication process is impractical. For most of our processes that involve high modal isolation, the coupler is fabricated to operate in a sufficiently adiabatic regime where small variations in L_0 and α become negligible. The parameters L_0 and α each affect the adiabaticity of the coupler in unique ways. Choosing their values involves balancing the need to maintain adiabaticity with the goal of keeping the device compact and durable. Additionally, practical constraints limit the allowable range for L_0. Since it impacts the overall length of the

OPTICS CONTINUUM

device, excessively large values of L_0 lead to overly long couplers that are too fragile. On the other hand, there is a minimum value for L_0, dictated by the length of the heating element (such as a flame, plasma arc, or filament). For each new type of PL, initial values are based on prior experience and are adjusted as needed to optimize the component without compromising its durability.

Modeling tools also present limitations, specifically regarding large wavelength bandwidths. Here, each curve plotting the adiabatic criteria vs logarithmic slope is calculated for a single wavelength, and a study over the whole range of intended performance is necessary before attempting to fabricate the device. In our numerical model, we employ a truncated modal basis consisting of a large number of guided-core and guided-clad eigenmodes. Although the continuous spectrum of leaky modes is not explicitly represented, this discrete set captures the dominant propagation dynamics within the taper. Moreover, the fiber assembly is housed inside a rigid capillary tube, whose boundary conditions further suppress any residual coupling to external leaky modes. Under these conditions, omitting the continuum of leaky modes introduces a negligible error in the predicted device performance. We did not show such an extensive set of curves in the main text, but an example is provided in the supplementary material (Supplement 1). We computed a large ensemble of guided-core and guided-clad eigenmodes (similar but with even more modes than Fig. S2 of supplementary material) but only plotted those exhibiting the strongest coupling to the fundamental mode, since higher-order modes—with diverging effective indices and increasingly orthogonal field symmetries—have overlap integrals that rapidly approach zero and thus contribute negligibly.

Even with simulation tools, the most comprehensive information about a component's performance is obtained by analyzing the full power transfer for each wavelength performance and its optical profile to determine its usefulness in any application. An important consideration when monitoring results is to avoid misinterpreting segregation as an absence of coupling.

Most of the fluctuations in power transfer observed with the same type of fiber (such as AAA, AAB, and ABB configurations) reflect the behavior of standard single-mode splitters or wavelength-division multiplexers. Factors that can influence power transfer include the degree of fusion, coupling length, taper shape, core spacing, effective refractive index, fiber configuration, and, in some cases, the characteristics of the source, such as its polarization. The coupling length needs to be taken into account as the tapered region is subsequently cut in half to make two devices from one fabrication sequence, and no amount of modeling can precisely determine the exact outcome. The performance of each device depends on its coupling efficiency, which is influenced by the effective refractive index of each fiber. Since each fiber has a different first cladding, the effective refractive index changes when the fiber is tapered. This change can break symmetry and selectively generate different modes. Therefore, while simulations provide an initial understanding, experimental characterization of each device is essential to account for any changes that might affect coupling efficiency, operational wavelength, and optical profile.

The far-field optical profiles only provide intensity information. Phase information is important to fully characterize the transverse modes, but its measurement is beyond the scope of this work.

On the other hand, while the AAB configuration demonstrates intriguing behavior, it is crucial to note that it could evolve into a MSPL by increasing the length of the final component. Figure 6(a) illustrates that, by creating a component that reaches values on the order of 10^{-5}, each mode can be individually generated in the few-mode section. Although this configuration may not yield a highly robust component, it does enable the development of a mode-selective component with a reduced number of fibers.

Finally, all PLs fabricated for this study were made with synthetic fused silica capillary tubes, which do not provide the best results in terms of excess loss. Better components can be manufactured using more expensive fluoride capillary tubes. With the exception of excess

OPTICS CONTINUUM

loss, fused silica capillaries allow reproducing the main outcomes obtained with more expensive capillary tubes.

6. Conclusion

This study identifies which of the model's variables allow predicting the type and specifications of manufactured PLs. Also, implementing double-clad fibers with single-mode compatibility with SMF28 enables optimal and real-time characterization of any PL type. This study paves the way for better reproducibility and manufacturing yields for various PLs. The study describes the properties of the various types of PLs to allow for a better adequacy between a device type and a particular application across various fields. For instance, pure improvements in light collection can be achieved with large bundles of standard PLs [17]. In contrast, purely MSPLs provide additional contrast in some imaging modalities such as optical coherence tomography [20]. Finally, semi-mode selective PLs will prove helpful in telecommunications, where degeneracy of the LP_{11} modes cannot be avoided over long distances in cylindrical symmetries [39].

Fabricating any type of PL for its implementation requires identifying their coupling performance, operational wavelength, and optical profile of the output. Therefore, the simulations and characterizations are critical for its implementation. Simulation tools allow for the determination of the essential ingredients needed for manufacturing devices with specific characteristics. This is particularly relevant when the modeling tool indicates no intersection between the adiabatic criteria and the logarithmic slope of the taper profile.

The existence of reliable models allows for the analysis of numerous new PLs designs without the need for lengthy trial-and-error manufacturing processes. Meanwhile, the fabrication process and characterization provide insights into the coupling performance, operational wavelength, and optical profile. These performance attributes can vary depending on the fiber type, length of the device, and fabrication procedure.

Additionally, ideally, it is possible to categorize PLs into three main types: 1. Conventional PLs, which exhibit strong coupling performance between each port, a high dependence on wavelength, and a superposition of guided modes. 2. Mode-selective devices provide high isolation between all modes, a broadband operational wavelength, and the generation of each mode individually. 3. Hybrid components, which combine the behaviors of the first two types—exhibiting high isolation between certain ports while maintaining strong coupling with others in a large bandwidth with a mixture in the profile of the mode.

Funding. HORIZON EUROPE European Research Council (101070700); Natural Sciences and Engineering Research Council of Canada (RGPIN-2018-06151).

Acknowledgment. The authors thank Mikaël Leduc for his invaluable work on the fabrication and characterization setup.

Disclosures. RIBD: Castor Optics, inc. (E), CB: Castor Optics, inc. (I), NG: Castor Optics, inc. (I,P).

Data availability. The data underlying the results presented in this paper is not publicly available at this time but may be obtained from the authors upon reasonable request.

Supplemental document. See Supplement 1 for supporting content.

References

1. T. A. Birks, I. Gris-Sánchez, S. Yerolatsitis, *et al.*, "The photonic lantern," Adv. Opt. Photonics **7**(2), 107–167 (2015).
2. C. Qiu, W. Ma, F. Liu, *et al.*, "A simplified mode diversity coherent receiver based on non-mode-selective photonic lantern and Kramers-Kronig detection," Opt. Laser Technol. **161**, 109229 (2023).
3. S. G. Leon-Saval, N. K. Fontaine, and R. Amezcua-Correa, "Photonic lantern as mode multiplexer for multimode optical communications," Opt. Fiber Technol. **35**, 46–55 (2017).
4. M. Jiang, C. Chen, B. Zhu, *et al.*, "Mimo-free WDM–MDM bidirectional transmission over OM3 MMF," Opt. Commun. **473**, 125988 (2020).
5. L. Jin, Y. Wang, M. Zhang, *et al.*, "Measurement of differential mode group delay in few-mode fiber with correlation optical time-domain reflectometer," Appl. Opt. **61**(13), 3579–3582 (2022).

OPTICS CONTINUUM

6. G. Li, N. Bai, N. Zhao, *et al.*, "Space-division multiplexing: the next frontier in optical communication," Adv. Opt. Photonics **6**(4), 413–487 (2014).
7. W. Chen, G. Hu, F. Liu, *et al.*, "Measurement of mode coupling distribution along few mode fiber based on two photonic lanterns," Opt. Commun. **428**, 136–143 (2018).
8. S. Swain and D. Venkitesh, "Evaluation of mode division multiplexed system by dynamic power transfer matrix characterization," OSA Continuum **3**(10), 2880–2892 (2020).
9. H. K. Chandrasekharan, F. Izdebski, I. Gris-Sánchez, *et al.*, "Multiplexed single-mode wavelength-to-time mapping of multimode light," Nat. Commun. **8**(1), 14080 (2017).
10. Z. Liu, S. Zhang, Z. Qian, *et al.*, "Intelligent few-mode multi-wavelength fiber laser based on photonic lantern comb filter," Opt. Laser Technol. **180**, 111501 (2025).
11. L. Zhang, L. Pei, J. Wang, *et al.*, "A gain-equalized FM-EDFA with gain clamping for burst-mode signals in MDM-PON," Opt. Laser Technol. **177**, 111180 (2024).
12. J.-C. Olaya, S. G. Leon-Saval, D. Schirdewahn, *et al.*, "1:61 photonic lanterns for astrophotometry: a performance study," Mon. Not. R. Astron. Soc. **427**(2), 1194–1208 (2012).
13. Y. J. Kim, M. P. Fitzgerald, J. Lin, *et al.*, "Spectral characterization of a three-port photonic lantern for application to spectroastrometry," J. Astron. Telesc. Instrum. Syst. **10**(04), 045004 (2024).
14. J. Lin, M. P. Fitzgerald, Y. Xin, *et al.*, "Focal-plane wavefront sensing with photonic lanterns II: numerical characterization and optimization," J. Opt. Soc. Am. **40**(12), 3196–3208 (2023).
15. T. Gu, F. Liu, Z. Huang, *et al.*, "Fiber Bragg grating sensing multiplexing method using photonic lantern spatial mode diversity," Opt. Commun. **574**, 131118 (2025).
16. Y. Lu, Z. Jiang, W. Liu, *et al.*, "Orbital angular momentum mode generation system based on photonic lantern," J. Opt. **21**(12), 125702 (2019).
17. I. Ozdur, P. Toliver, A. Agarwal, *et al.*, "Free-space to single-mode collection efficiency enhancement using photonic lanterns," Opt. Lett. **38**(18), 3554–3557 (2013).
18. M. Salit, J. Klein, and L. Lust, "Experimental characterization of a mode-separating photonic lantern for imaging applications," Appl. Opt. **59**(17), 5319–5324 (2020).
19. R. Maltais-Tariant, R. I. Becerra-Deana, S. Brais-Brunet, *et al.*, "Speckle contrast reduction through the use of a modally-specific photonic lantern for optical coherence tomography," Biomed. Opt. Express **14**(12), 6250–6259 (2023).
20. M. Poinsinet de Sivry-Houle, S. B. Beaudoin, S. Brais-Brunet, *et al.*, "All-fiber few-mode optical coherence tomography using a modally-specific photonic lantern," Biomed. Opt. Express **12**(9), 5704–5719 (2021).
21. D. Choudhury, D. K. McNicholl, A. Repetti, *et al.*, "Computational optical imaging with a photonic lantern," Nat. Commun. **11**(1), 5217 (2020).
22. S. G. Leon-Saval, T. A. Birks, J. Bland-Hawthorn, *et al.*, "Multimode fiber devices with single-mode performance," Opt. Lett. **30**(19), 2545–2547 (2005).
23. L. Xu, L. Pei, J. Wang, *et al.*, "Synthetic photonic lantern characterization and power regulation with intensity superposition mode decomposition," Opt. Express **32**(13), 22663–22674 (2024).
24. L. Shen, L. Gan, C. Yang, *et al.*, "Highly mode selective 3-mode photonic lantern through geometric optimization," in *Optical Fiber Communication Conference (2018)*, paper W2A.14, (2018), p. W2A.14.
25. S. Sunder and A. Sharma, "Adiabatic propagation algorithm for photonic lanterns," Opt. Fiber Technol. **57**, 102219 (2020).
26. D. Yu, S. Fu, Z. Cao, *et al.*, "Mode-dependent characterization of photonic lanterns," Opt. Lett. **41**(10), 2302–2305 (2016).
27. N. K. Fontaine, J. Carpenter, S. Gross, *et al.*, "Photonic lanterns, 3-D waveguides, multiplane light conversion, and other components that enable space-division multiplexing," Proc. IEEE **110**(11), 1821–1834 (2022).
28. S. G. Leon-Saval, N. K. Fontaine, J. R. Salazar-Gil, *et al.*, "Mode-selective photonic lanterns for space-division multiplexing," Opt. Express **22**(1), 1036–1044 (2014).
29. A. M. Velázquez-Benítez, J. E. Antonio-López, J. C. Alvarado-Zacarías, *et al.*, "Scaling photonic lanterns for space-division multiplexing," Sci. Rep. **8**(1), 8897 (2018).
30. F. Anelli, A. Annunziato, A. M. Loconsole, *et al.*, "Mode-group selective photonic lantern based on indium fluoride optical fibers for mid-infrared," J. Lightwave Technol. **43**(1), 280–287 (2025).
31. J. Yamauchi, T. Ando, and H. Nakano, "Beam-propagation analysis of optical fibres by alternating direction implicit method," Electron. Lett. **27**(18), 1663–1665 (1991).
32. A. Sharma and S. Banerjee, "Method for propagation of total fields or beams through optical waveguides," Opt. Lett. **14**(1), 96–98 (1989).
33. J. Bures, *Guided Optics: Optical Fibers and All-Fiber Components* (Wiley-VCH, 2008).
34. S. Chen, Y. ge Liu, Z. Wang, *et al.*, "Mode transmission analysis method for photonic lantern based on fem and local coupled mode theory," Opt. Express **28**(21), 30489–30501 (2020).
35. X. Zhou, "Optimization design of mode-selective ring core photonic lantern based on coupled local mode theory," Opt. Commun. **553**, 130120 (2024).
36. M. Poinsinet de Sivry-Houle, R. I. Becerra-Deana, S. Virally, *et al.*, "Supymode: an open-source library for design and optimization of fiber optic components," Opt. Continuum **3**(2), 242–255 (2024).
37. M. Poinsinet de Sivry-Houle, "Martinpdes/supymode: 1.0.0," (2023).

OPTICS CONTINUUM

38. T. Birks and Y. Li, "The shape of fiber tapers," J. Lightwave Technol. **10**(4), 432–438 (1992).
39. R. I. Becerra-Deana, M. P. de Sivry-Houle, S. Virally, *et al.*, "Mode-selective photonic lanterns with double-clad fibers," J. Lightwave Technol. (to be published).

132.207.4.76 2025-11-18 15:01:40